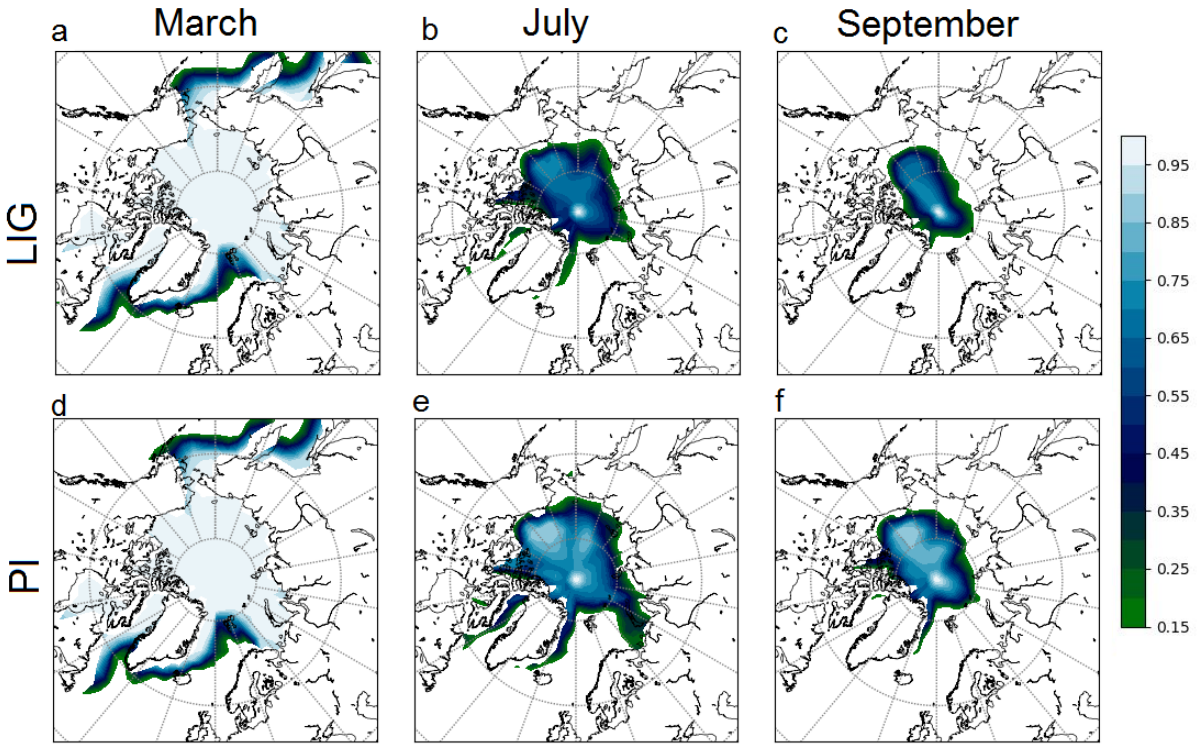
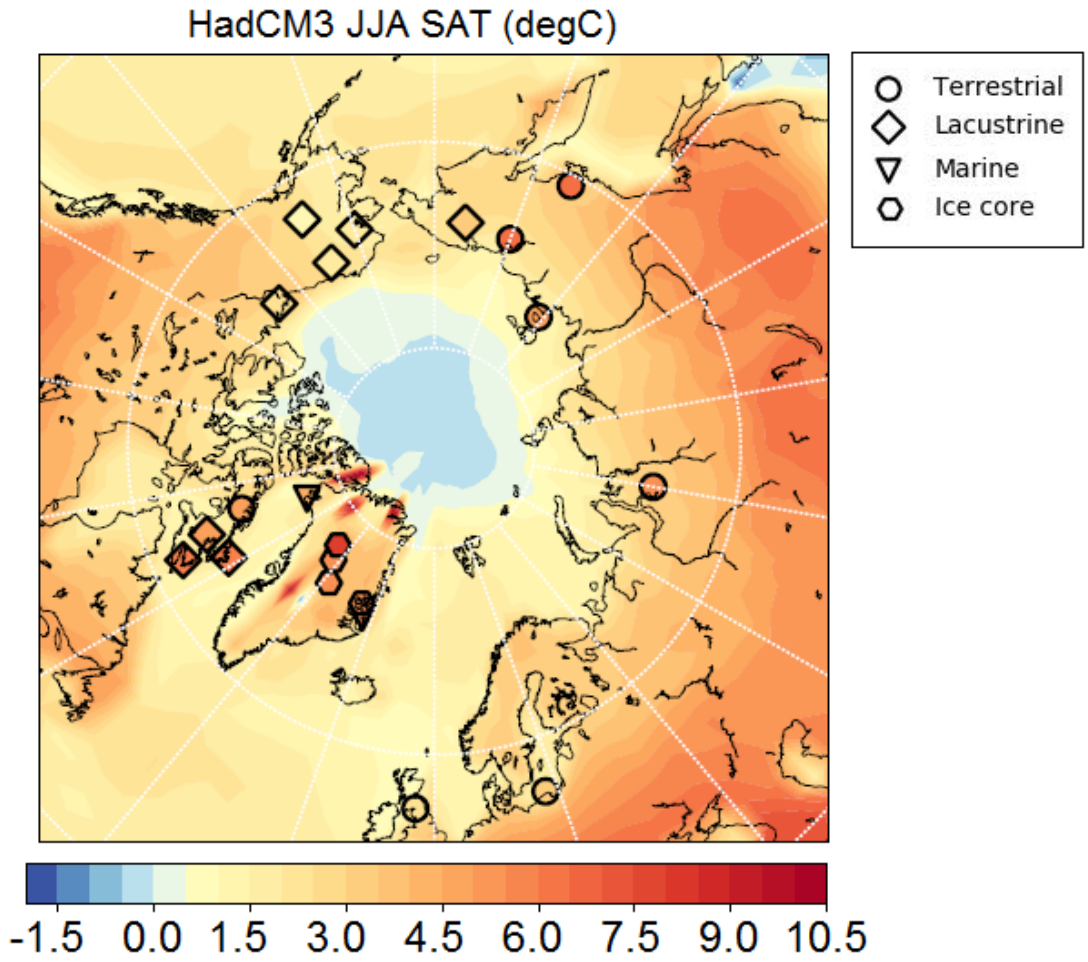
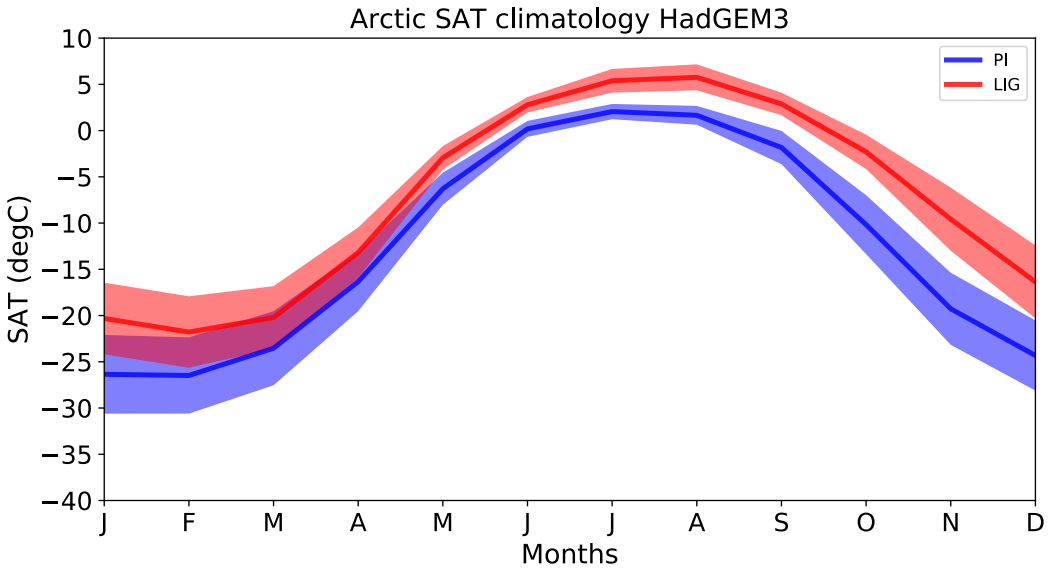
Sea ice-free Arctic during the Last Interglacial supports fast future loss



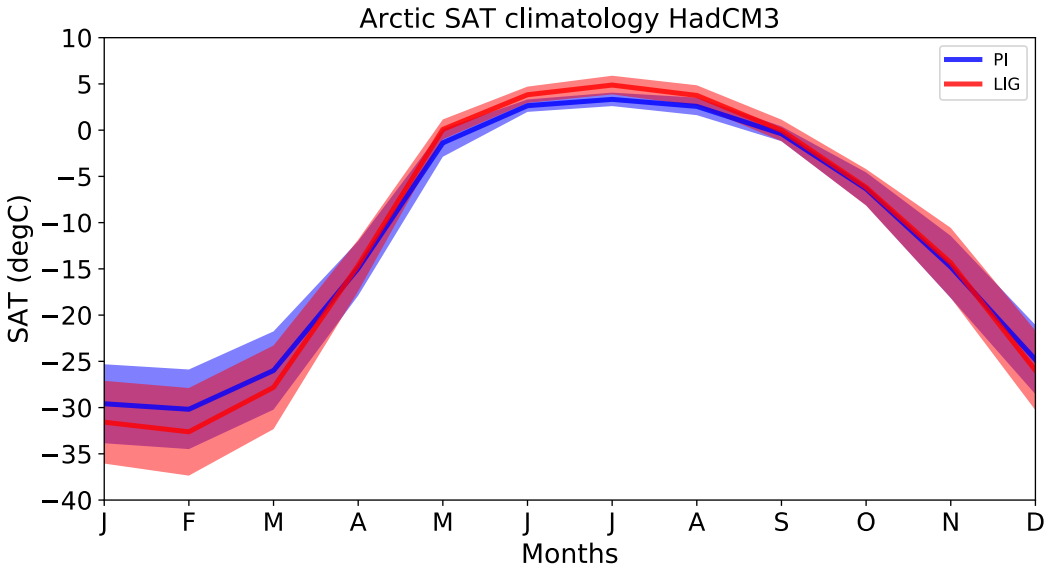
Supplementary Figure 1 Simulated HadCM3 March, July and September 50-year means of sea ice concentration for LIG (a,b,c) and PI (d,e,f).



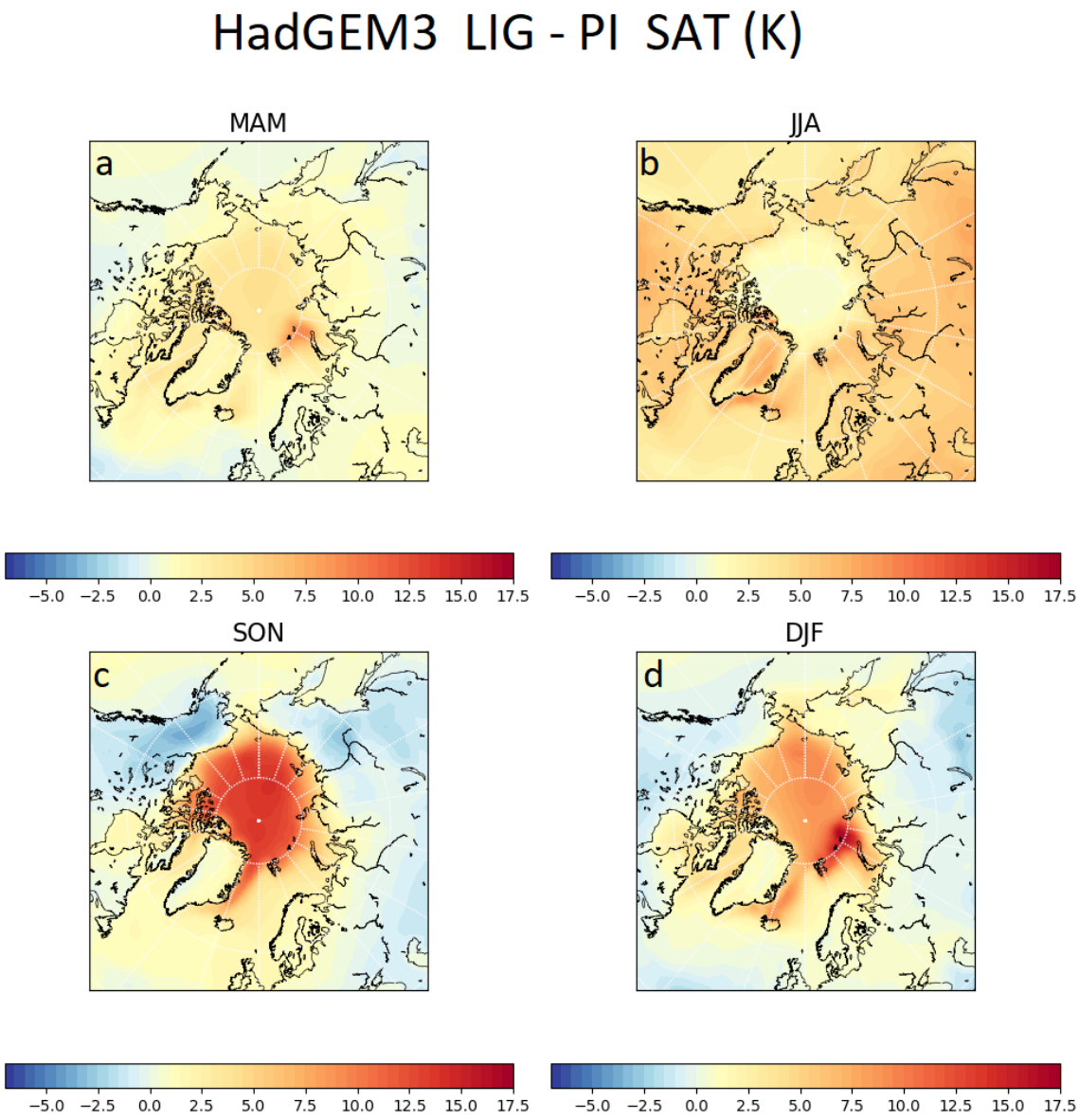
Supplementary Figure 2 HadCM3 summer (JJA) LIG - PI surface air temperature anomalies overlain by maximum LIG summer temperature anomalies relative to preindustrial era derived from paleotemperature proxies.



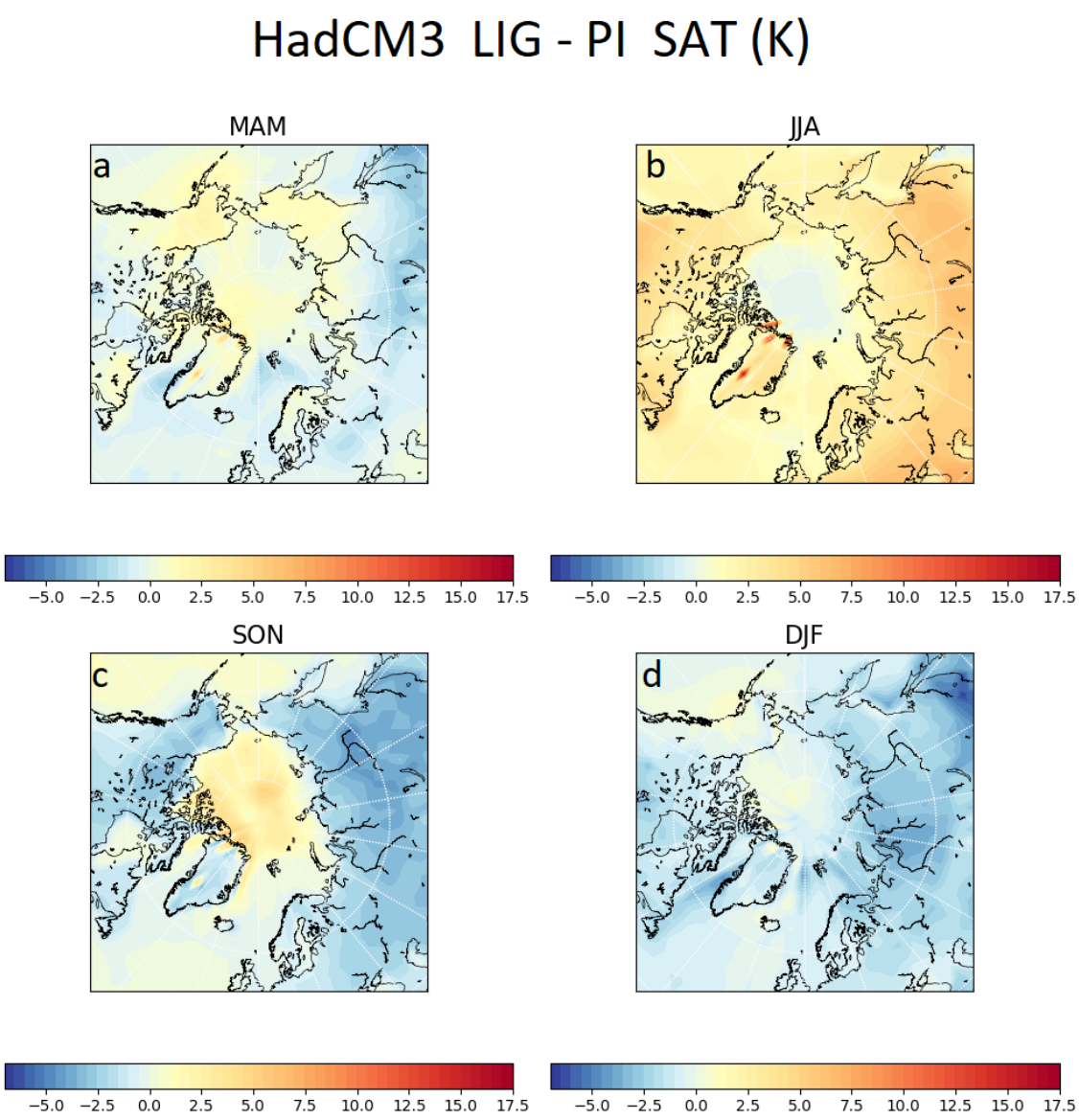
Supplementary Figure 3 HadGEM3 monthly Arctic (70 – 90 N) SAT climatology for LIG (red line) and PI (blue line). Thick lines represent the long-term means, shades represent ± two times the standard deviation.



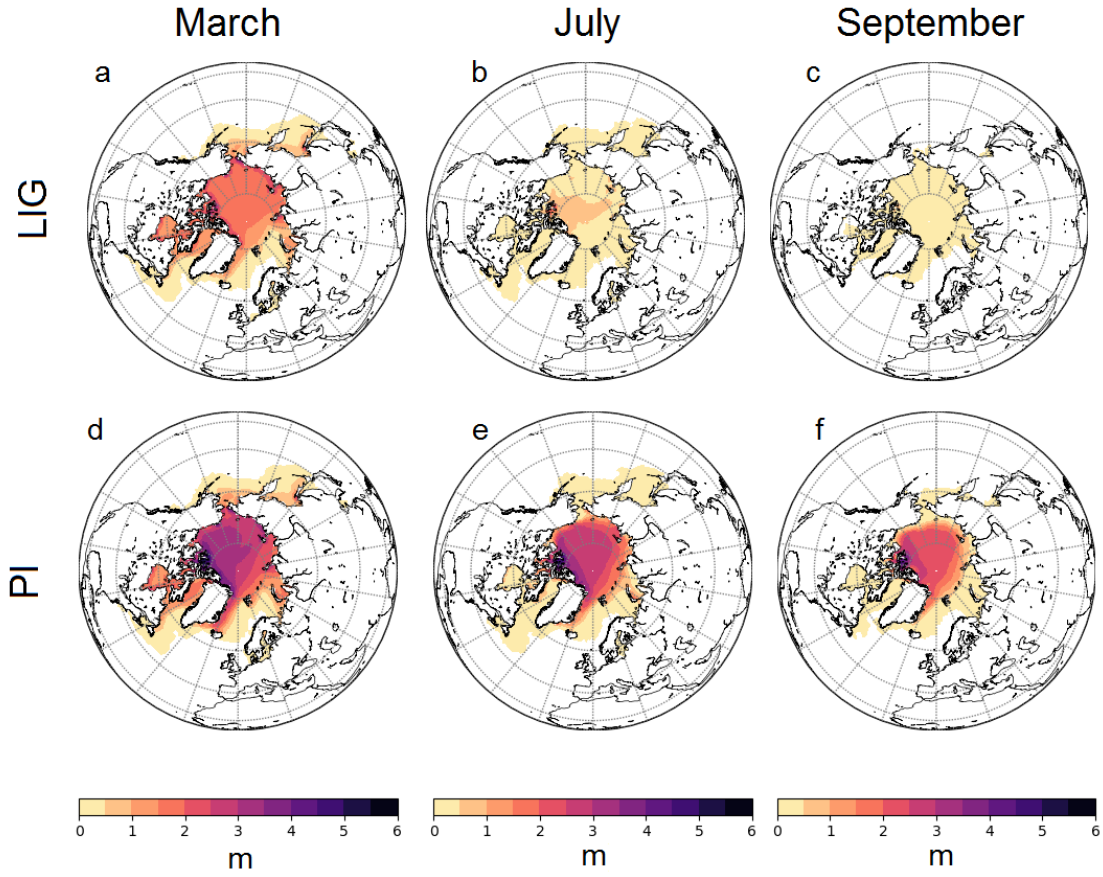
Supplementary Figure 4 as in Suppl. Figure 3 but for HadCM3.



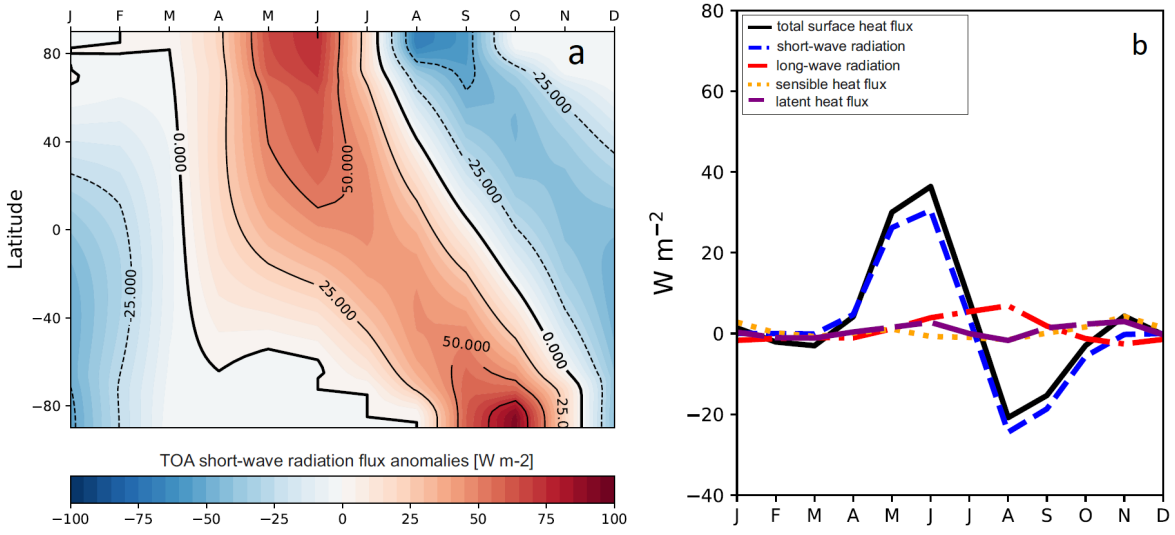
Supplementary Figure 5 SAT LIG – PI anomalies for all seasons as simulated by the HadGEM3 model.



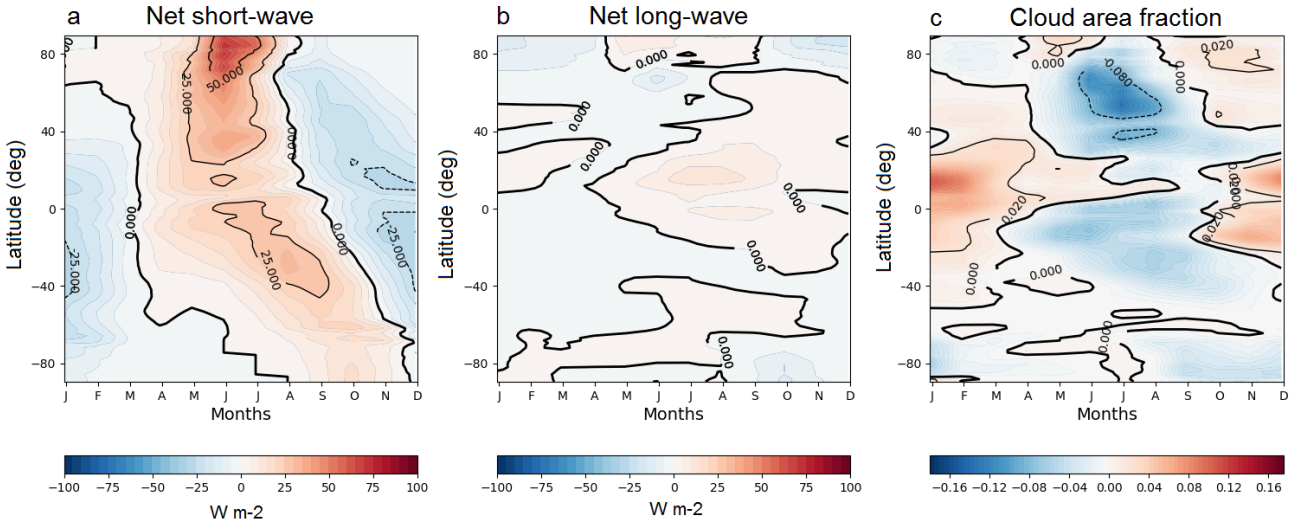
Supplementary Figure 6 as in Suppl. Figure 5 but for HadCM3.



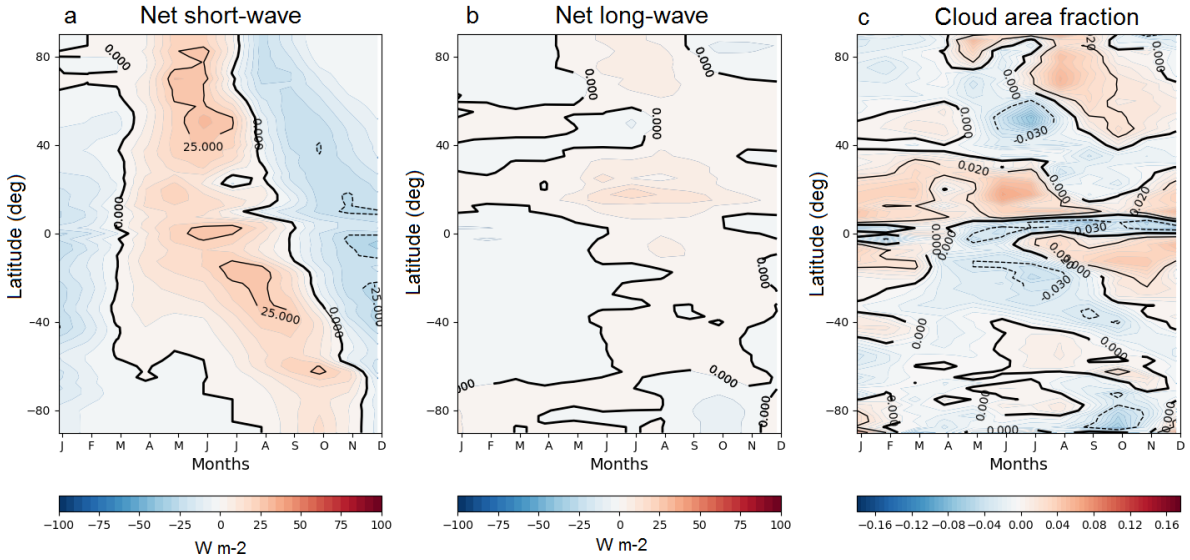
Supplementary Figure 7 March, July and September 200-year means of sea ice thickness for LIG (a,b,c) and PI (d,e,f) as simulated by the HadGEM3 model.



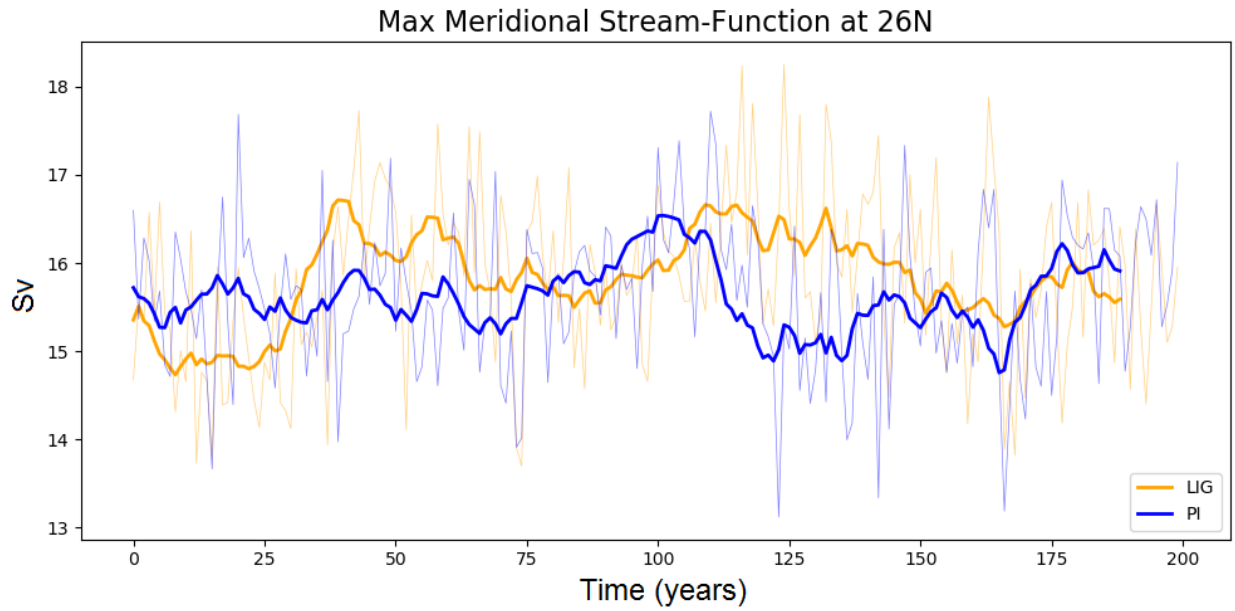
Supplementary Figure 8 As in Figure 3 but for HadCM3. (a) Monthly zonal-mean LIG - PI anomalies of the Top of Atmosphere (TOA) short-wave incoming radiation for the HadCM3 model. (b) LIG - PI anomalies for each term of the surface energy budget computed between 70N and 90N for the HadCM3 model.



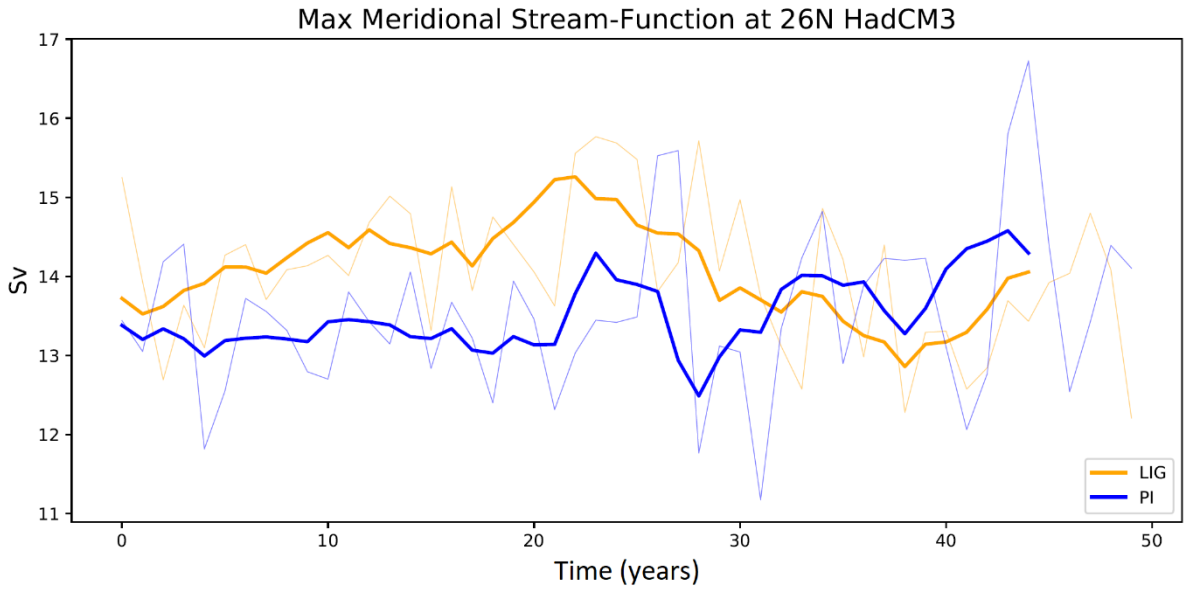
Supplementary Figure 9 Monthly zonal-mean LIG - PI anomalies of (a) net short-wave radiation flux at the surface, (b) net long-wave radiation flux at the surface and (c) cloud area fraction (total column) for the HadGEM3 model. Note that the characteristic LIG dipole of top-of-atmosphere positive (JAS)/negative (SON) incoming radiation anomaly in summer and spring (see Fig. 3a) disappears when the short-wave incoming radiation is evaluated at the surface (Suppl. Fig. 9a). During the LIG, the loss of summer sea ice drastically decreases the albedo in the Arctic region. As a consequence, more radiation is able to reach the ocean. This process compensates the negative top-of-atmosphere SW radiation anomaly in SON during the LIG (Fig. 3a), and the resulting SON LIG-PI net SW radiation anomaly at the surface is approximately zero (Suppl. Fig. 9a).



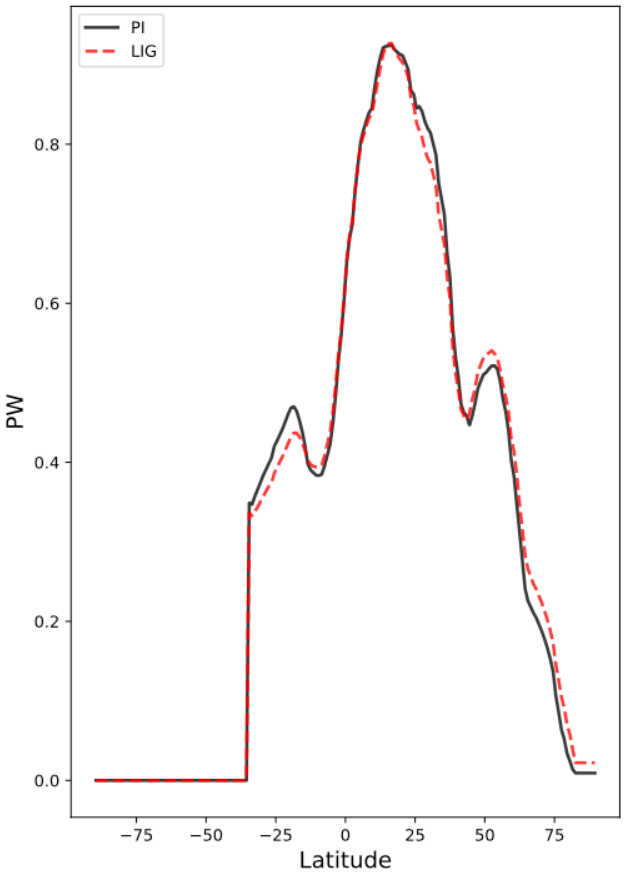
Supplementary Figure 10 as in Suppl. Figure 9 but for HadCM3.



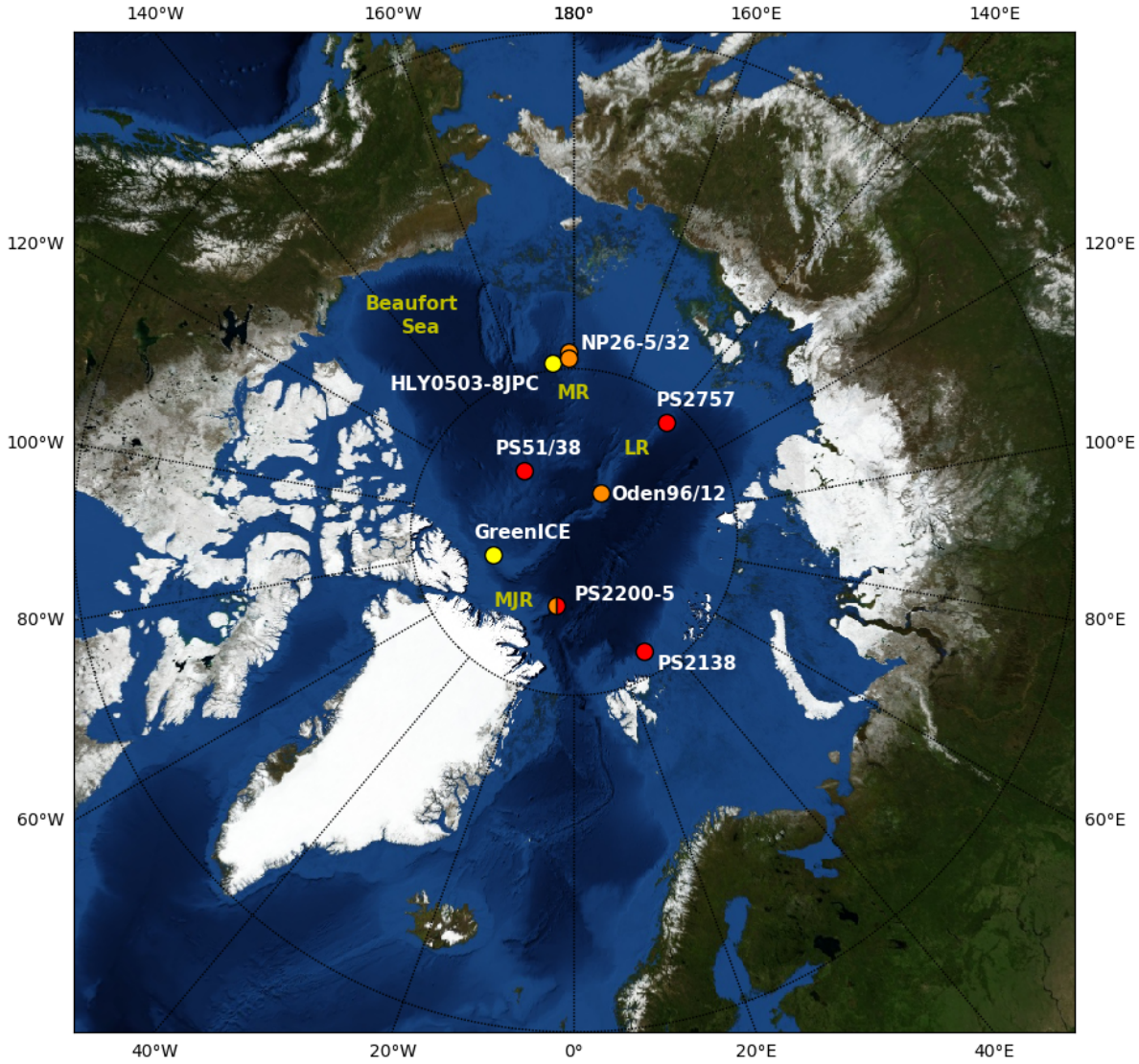
Supplementary Figure 11 Maximum northward volume transport of the Atlantic meridional overturning circulation at 26N for LIG (orange line) and PI (blue line). Thin lines represent annual means, thick lines represent a 11-year running mean.



Supplementary Figure 12 As in Suppl. Figure 11 but for HadCM3.



Supplementary Figure 13 Advective oceanic heat transport in the Atlantic basin for the LIG (red dashed line) and PI (black line) HadGEM3 simulations. 200-year means are used.



Supplementary Figure 14 Map showing the location of observations of LIG Arctic sea ice changes based on ostracode faunas (orange circles - Cronin et al., 2010), subpolar foraminifers (yellow circles - Nørgaard-Pedersen et al., 2007; Adler et al., 2009), and biomarker proxy IP25 (red circles - Stein et al., 2017). Locations of the Morris Jesup Rise (MJR), Lomonosov Ridge (LR) and Mendeleyev Ridge (MR) sites are also shown.

MODEL SPECIFICATIONS	HADGEM3-GC3.1_LL	HADCM3
EARTH SYSTEM COMPONENTS	Atmosphere: UM (ENDGame) Land: JULES (4.8) Ocean: NEMO (3.6) Sea ice: CICE (5.2)	Atmosphere: HadAM3 Land: MOSES Ocean: HadOM3 Sea Ice: HadOM3
GRID SPACING	Atmosphere ~140 km Ocean: ~ 100 km	Atmosphere: ~300 km Ocean: ~ 125km
HORIZONTAL GRID - ATMOSPHERE	Latitude-longitude grid with Arakawa-C staggering	Latitude-longitude grid with Arakawa-B staggering
HORIZONTAL GRID - OCEAN	Curvilinear orthogonal grid (ORCA 1) with Arakawa-C staggering	Latitude-longitude grid with polar island
MODEL VERTICAL LEVELS	Atmosphere: 85 Ocean: 75	Atmosphere: 19 Ocean: 20
HYDROSTATIC	NO	YES
SEA ICE SCHEME		
THERMODYNAMICS	• four sea ice layers and one snow layer with heat capacity depending on temperature and salinity based on Bitz and Lipscomb (1999). Surface exchange calculations carried out separately for five ice thickness categories. • Prognostic melt pond scheme (Flocco et al., 2012).	• Zero-layer model of Semtner (1976). • Temperature dependent surface albedo to account for the ageing of snow, the formation of melt ponds, and the relatively low albedo of bare ice.
DYNAMICS	• Elastic–viscous–plastic rheology with remapping algorithm scheme for transport/advection (Hunke et al., 2015). • ORCA1 grid	• Simple scheme from Bryan (1969) applying the wind stress to the ocean beneath the ice and using the top layer ocean current for advection. • No sea ice rheology, no convergence above threshold ice thickness value of 4m. • Latitude-longitude grid with polar island

Supplementary Table 1 HadGEM3 vs HadCM3 general model specifications and description of the sea ice schemes employed by the two models. For the HadGEM3 sea ice scheme see Ridley at al. 2018 and for the HadCM3 sea ice scheme see Gordon et al. 2000.

Lat, Lon	Site	Observation type	Observations (K)	HadGEM3 (K)	HadCM3(K)
Terrestrial					
55, 18	Europe	Terrestrial: pollen, plant macrofossils	3.4 ± 0.5*	4.3 ± 1.2	1.5 ± 1.8
55, -3	UK	Terrestrial: Pollen, plant macrofossils	2.4 ± 0.5*	3.5 ± 1.0	1.9 ± 1.0
61, 152.5	Magadan	Terrestrial: pollen	6.4 ± 2	4.5 ± 1.4	3.7 ± 2
68, 80	West-central Siberia	Terrestrial: pollen, plant macrofossils	5.4 ± 2	6.4 ± 2.1	3.4 ± 2.3
68, 160	Northeast Siberia	Terrestrial: pollen	6.4 ± 2	4.4 ± 2.0	2.1 ± 1.8
70, -72.5	Flitaway	Terrestrial: insects, plant remains	4.9 ± 0.5	5.8 ± 1.7	2.4 ± 1
73.33,141.5	bolshoy lyadhovshy	Terrestrial: pollen	4.9 ± 0.5	3.1 ± 1.6	1.2 ± 1.3
Lacustrine					
63, -66	Robinson Lake	Lacustrine: pollen	5.4 ± 0.5*	5.4 ± 1.4	1.0 ± 1.2
64, -150	Birch Creek/ky11	Lacustrine: pollen	1.4 ±1	3.6 ± 1.4	2.4 ± 1.6
66, -69.2	Amarok Lake	Lacustrine: pollen	4.9 ± 0.5	5.8 ± 1.9	1.3 ± 1
67, -160	Squirrel Lake	Lacustrine: pollen, plant Macrofossils	1.9 ± 1.5	3.5 ± 1.8	1.7 ± 1.7
67, -62	Cumber	Lacustrine: pollen	5.9 ± 1.5	5.1 ± 1.2	1.5 ± 0.9
67.5,172.08	Lake Elgygytgyn	Lacustrine: pollen	3.4 ± 1	4.7 ± 1.7	2.5 ± 1.6
69, -151	Ahaliorak Lake	Lacustrine: pollen	1.9 ± 1.5	4.3 ± 1.9	2.6 ± 1.6
69, -133	Lake Tuk 5	Lacustrine: plant macrofossils, beetles	2.4 ± 0.5*	4.5 ± 2.3	3.3 ± 2
Marine					
71.75, -23	Jameson	Marine: pollen, plant macrofossils,	5.4 ± 0.5*	4.4 ± 1.2	2.4 ± 1.4

		beetles, other invertebrates			
76.35, -68.3	Thule	Marine: pollen, chironomids	4.4 ± 0.5*	5.1 ± 1.4	1.2 ± 0.8
Ice Core					
73, -25	Renland	Ice core: d18O, dD	5.4 ± 0.5*	3.8 ± 1.0	3.3 ± 1.3
73, -38	GISP2	Ice core: d18O, dD	5.4 ± 0.5*	6.9 ± 1.5	3.6 ± 1.2
75, -42	NGRIP	Ice core: d18O, dD	5.4 ± 0.5*	7.0 ± 1.5	3.3 ± 1.4
76.4, -44.8	NEEM_ds	Ice core: d18O, dD	8 ± 4	7 ± 1.5	4 ± 1.3
			4.5 ± 1.7	**4.9 ± 1.2**	**2.4 ± 0.9**

Supplementary Table 2 Comparison between observational data for the peak LIG warmth relative to preindustrial era (and past millennium for NEEM[3]) and modelled JJA LIG - PI surface air temperature anomalies for the HadGEM3-GC3.1 and HadCM3 models. For each site, mean and standard deviation are show. The last row shows mean and associated standard deviation computed across sites. Green shading indicates model-observation agreement within the uncertainty ranges, red shading indicates model-observation disagreement. Original datasets are from Kaspar et al., 2005 , CAPE, 2006, and Capron et al., 2017. Note, however, that for consistency with modelled data, the original temperature observations for all sites (except for NEEM) were corrected to take into account a warming of 0.4 K between preindustrial and present day (1961-1990) conditions (Turney and Jones, 2010). See Methods for further details.

*For these sites, the standard deviation of the temperature data is not available. To take into account data uncertainty (which must exist), a standard deviation of ± 0.5 was used. This is the smallest standard deviation found in any proxy record across all sites. It allows us to make a conservative estimation of the uncertainty associated to proxy data, where unknown, without making additional assumptions on the upper boundary of the magnitude of the uncertainty. If the model-observation agreement is computed using the original data, with no standard deviation for a few sites HadGEM3 matches 85% of the data (instead of 95% when a standard deviation of ± 0.5 is considered) and HadCM3 matches 42% of the data (instead of 47%).

CMIP3	ECS (K)	ICE FREE	CMIP5	ECS (K)	ICE FREE	CMIP6	ECS (K)	ICE FREE
CCSM3	2.7	2044	**ACCESS1.0**	3.8	2027	**CNRM-CM6-1**	4.8	2060
CGCM3.1 (T47)	3.4	NA	**BCC–CSM1.1**	2.8	NA	**CESM2**	5.2	2038
CGCM3.1 (T63)	3.4	NA	**BCC–CSM1.1**	2.9	NA	**UKESM1_LL**	5.3	2038
CSIRO-MK3.0	3.1	NA	**BNU–ESM**	4.1	2028	**HadGEM3-GC3.1**	5.5	2035
ECHAM5/ MPI-OM	3.4	2081	**CanESM2**	3.7	2020	**IPSL-CM6A-LR**	4.5	2029
ECHO-G	3.2	2077	**CCSM4**	2.9	2065	**MIROC 6**	2.6	2063
FGOALS-G1.0	2.3	NA	**CNRM–CM5**	3.3	2032	**CESM2-WACCM**	4.7	2038
GFDL-CM2.0	2.9	NA	**CSIRO–Mk3.6.0**	4.1	NA	**CanESM5**	5.6	2038
GFDL-CM2.1	3.4	2042	**GFDL–CM3**	4	2039	**GFDL-CM4**	3.9	2055
GISS-EH	2.7	NA	**GFDL–ESM2G**	2.4	2076	**MPI-ESM1-2-HR**	2.9	2050
GISS-ER	2.7	NA	**GFDL–ESM2M**	2.4	2057	**EC-earth3-Veg**	4.3	2053
INM-CM3.0	2.1	2040	**GISS–E2–H**	2.3	NA	**NESM3**	4.7	2066
IPSL-CM4	4.4	2066	**GISS–E2–R 2**	2.1	2030			
MIROC3.2 (HIRES)	4.3	NA	**HadGEM2–ES**	4.6	2048			
MIROC3.2 (MEDRES)	4	2067	**INM–CM4**	2.1	NA			
MRI-CGCM2.3.2	3.2	NA	**IPSL–CM5A–LR**	4.1	2059			
PCM	2.1	NA	**IPSL–CM5B–LR**	2.6	2081			
UKMO-HADCM3	3.3	2086	**MIROC5**	2.7	2060			
UKMO-HADGEM1	4.4	2063	**MIROC–ESM**	4.7	2033			
			MPI–ESM–LR	3.6	2051			
			MPI–ESM–P	3.5	NA			
			MRI–CGCM3	2.6	2051			
			NorESM1–M	2.8	2066			
	3.2±0.7	**2062±17**		**3.2±0.8**	**2048±18**		**4.5±0.9**	**2046±12**

Supplementary Table 3 Equilibrium Climate Sensitivity (ECS) and first year of September sea ice disappearance for CMIP3, CMIP5 and CMIP6 models. Note that for CMIP3 and CMIP5 only models for which ECS is known, according to AR4 and AR5, are shown. For CMIP6, ECS and ice-free year have been calculated using all models currently available on the Earth System Grid Federation (ESGF) (see Methods for details). The last row shows the mean and associated standard deviation for ECS and year of ice disappearance across all models.

ASTRONOMICAL PARAMETERS	**LIG**	**PI**
ECCENTRICITY	0.039378	0.016764
OBLIQUITY	24.040°	23.459°
PERIHELION-180°	275.41°	100.33°
DATE OF VERNAL EQUINOX	March 21 at noon	March 21 at noon
TRACE GASES		
CO_2	275 ppm	284.3 ppm
CH_4	685 ppb	808.2 ppb
N_2O	255 ppb	273 ppb

Supplementary Table 4 Astronomical parameters and atmospheric trace gas concentrations used in HadGEM3 and HadCM3 LIG and PI simulations.